AIChE WILEY InterScience DISCOVER SOMETHING GREAT

FLUID MECHANICS AND TRANSPORT PHENOMENA

Mass Transport Enhancement in the DMFC Using an Externally Applied Oscillatory Flow

Philip P. Schonewill and David T. Leighton Jr.
Dept. of Chemical and Biomolecular Engineering, University of Notre Dame, Notre Dame, IN 46556

DOI 10.1002/aic.11453
Published online April 22, 2008 in Wiley InterScience (www.interscience.wiley.com).

The direct methanol fuel cell experiences performance decay at high current densities due to mass transfer limitations. The dominant mass transfer limiting mechanism at high methanol/water feed rates and low methanol feed concentrations has been attributed to the slow diffusion of methanol through the porous diffusion layer of the anode. In this study, fluid oscillations were induced in the feed to the anode of a DMFC and significant performance improvements were observed at high current densities. It was found that the improvement in measured limiting current densities over steady flow operation was as large as twofold and the peak power density increased by as much as 30%. A model is presented which predicts the experimental values of limiting current density as a function of the Peclet number in the porous diffusion layer of the DMFC anode. © 2008 American Institute of Chemical Engineers *AIChE J,* 54: 1410–1423, 2008

Keywords: mass transfer, fuel cells, porous media, energy

Introduction

Direct methanol fuel cells (DMFCs) are a promising alternative to hydrogen-fed fuel cells, having the advantages of a simpler overall design and a fuel that is easier to store and distribute. The basic reactions and operation principles of a DMFC have been studied extensively[1,2] and are illustrated in Figure 1. Several technical challenges with DMFCs still remain unresolved, including maximum power densities that are typically only a fraction of hydrogen-fed cells, crossover of methanol through the membrane to the cathode, and management of evolved carbon dioxide gas in the anode fuel stream.

Another problem which typically arises during DMFC operation is the poor mass transport of methanol to the DMFC anode at high current densities. The poor mass transport is indirectly due to the phenomenon of methanol crossover. Methanol permeates across the membrane and produces a mixed potential at the cathode, inhibiting the oxygen reduction reaction and resulting in a drop in the power output of the DMFC.[3] To avoid experiencing significant methanol crossover and the corresponding efficiency loss, the feed concentration of methanol is kept low (typically < 2 mol L^{-1}). Consequently, at high current densities when the reaction rate at the anode is fast enough to instantaneously consume any methanol that arrives at the catalyst surface, DMFC performance is limited by the inability of methanol to diffuse to the surface fast enough. Similarly, carbon dioxide diffuses slowly away from the catalyst surface, which tends to restrict methanol's access to reaction sites.

The effect of poor mass transport is evident when the current-voltage behavior of a DMFC is examined. The DMFC operates in three different regimes depending on the current density. The general features of this behavior are illustrated in Figure 2. At low current densities (region 1), kinetic limitations of the cell dominate. An approximately linear voltage-current relationship (region 2) occurs at moderate current densities. At high current densities (region 3), the mass transport resistances of the system limit performance. Eventually, these resistances become dominant and the cell voltage drops to zero at the limiting current density i_{lim}. Mass transport limitations are often explained by a combination of two phenomena: the presence of greater amounts of carbon dioxide (CO_2) gas in the anode flow channel and diffusion layer at high current densities, and diffusion of methanol into and

Correspondence concerning this article should be addressed to D. T. Leighton, Jr. at dtl@nd.edu.

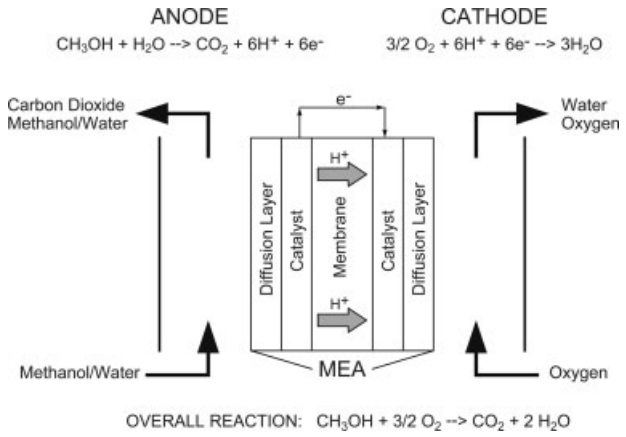

Figure 1. General schematic and reactions of the DMFC.

through the porous diffusion layer. Bubbles of CO_2 both physically block access to the catalyst surface and hydrodynamically influence the movement of liquid methanol fuel into pores.[4] The tendency for CO_2 gas to evolve and then coalesce into long slugs at high current densities and reduce i_{lim}, has been verified by analytical modeling[5] and visualization experiments.[6,7] Separate work[4,8–11] has suggested that the slow diffusion of methanol to the catalyst surface is also an important mass transport limiting mechanism, particularly when the methanol concentration is low. Despite these studies, how these two mass transfer limiting mechanisms interact with one another is not clear.

An operational technique used to counter mass transfer limitations is to increase methanol concentration in the feed, thereby increasing the concentration gradient across the porous diffusion layer. This practice is undesirable because it results in a higher rate of methanol crossover at lower current densities.[3,12] Another common approach is to increase the anode feed rate. This has been shown to positively[13,14] and negatively[4,7] affect the performance of a DMFC in the mass transfer limiting regime, depending on other operating conditions. In general, however, this practice is also not preferable because the increased flow rates reduce the cell temperature (if the anode feed is not preheated) and poorly utilize the fuel. Since methanol crossover is a more serious performance limitation in the DMFC, increasing the flow rate while keeping the methanol concentration below 2 mol L^{-1} is currently the best operational strategy to reduce mass transfer limitations.

In addition to operational changes, work has been performed which studies the effect of either the geometry of the anode flow field[15–17] or the porous diffusion layer.[18–22] In the case of the flow field, it was found that an optimum channel depth and orientation exists[15] and that a serpentine channel performed best in a DMFC.[16] Even in a case where a modified serpentine flow field improved DMFC mass transfer behavior, significant mass transfer limitations were still present.[17] For the diffusion layer, it was found that treating diffusion layers with Teflon did not improve performance beyond that of an untreated diffusion layer,[18,20,22,23] but that the thickness and microstructure of the layer does affect performance, especially at low methanol concentrations.[19–21] A good indicator of mass transfer behavior in the DMFC is the limiting current, and in general, improvements in the limiting current density were not significant in any of these studies.

In this article, we examine the effect of superimposing oscillatory flow on the steady feed to the anode of a DMFC. Oscillatory flow is an attractive alternative to increase the steady feed rate because it does not require additional fuel or preheating to maintain operating temperatures. As we shall demonstrate, the oscillatory flow generates a pressure gradient throughout the porous anode which induces convection within its pores. The convection promotes increased sampling of streamlines by solutes and can significantly improve mass transfer. Previous work[24,25] has demonstrated that oscillatory flow in a porous media significantly enhances the rate of mass transfer of solutes in the direction of the flow. It is this effect we expected to replicate, with the important distinction that the oscillatory flow in these experiments is perpendicular to the direction in which the solutes diffuse rather than in the flow direction. Hence, convective enhancement of mass transfer rates in the transverse direction should result in improvements in DMFC performance at high current densities.

In the next section, we examine how fluid oscillations affect mass transfer in an idealized DMFC and develop a predictive model for the limiting current density. In the third section, the experimental system and the methods used to measure DMFC performance are described. In the fourth section, the data from the experiments is presented. In the final section, an argument is made for methanol diffusion being the primary mass transport limiting mechanism in our experiments. Additionally, the model is compared to the data and some concluding remarks are made about the implications of this work.

Theory and Calculations

Model description and development

To enhance mass transport in the diffusion layer without significantly altering operational and geometric variables in the DMFC, it is necessary to induce convection in the pores

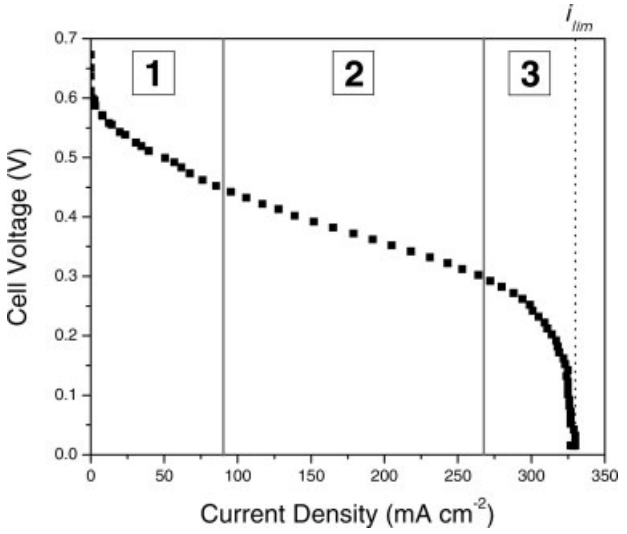

Figure 2. An example of a polarization curve obtained during this study at a cell temperature of 70°C that illustrates the three typical regions of behavior observed in DMFCs.

of the diffusion layer. In this work, convection is induced by displacing a known volume ΔV of fluid at a frequency ω, which forces an oscillatory flow. Inducing an oscillatory flow in the anode of a DMFC will affect momentum, mass, and energy transfer in the system. Characterizing these changes, however, is difficult because the transport behavior is complex. For instance, the anode geometry is complicated: the flow channel only exposes approximately 60% of the active catalyst area, and thus methanol transport may not be strictly one-dimensional and could be augmented by seeping through the porous diffusion layer underneath the ribs of the flow channel.[14,26] Additionally, in typical operation, the methanol/water solution is fed at ambient temperature and the cell temperature is more than 30°C higher, so temperature gradients are present in the fluid. Furthermore, due to the evolution of CO_2 gas, the solution becomes multiphase, most significantly at high current densities. Many efforts have been made to model the complexities of the transport behavior in the DMFC anode,[27] but for the purposes of this study, a simplified model that still captures the essence of the transport behavior at the low methanol feed concentrations considered here is desirable.

The following assumptions were made to isolate the effect of fluid oscillations on DMFC performance:

(1) Steady state, in the sense that the oscillatory flow is purely sinusoidal and all other transients are small in magnitude;

(2) Transport of methanol through the channel, porous medium, and catalyst layer is approximated as one-dimensional;

(3) The system is isothermal at the cell temperature;

(4) The anode feed solution is dilute in methanol;

(5) Fluid properties (μ, ρ) at the anode are constant;

(6) All carbon dioxide present in the porous diffusion layer is dissolved in solution.

With these assumptions in hand, we consider a simplified geometry of the DMFC anode such as the one presented in Figure 3.

As indicated by Figure 3, the anode channel has a depth d and the interaction of the fluid with the side walls is neglected, which reduces the important physical mechanisms to two: unidirectional flow in the x direction and diffusion of solutes in the y direction. The assumption of one-dimensional diffusion through the diffusion and catalyst layers requires the fluid in the open anode channel to be regarded as well-mixed at the inlet feed concentration. This will be correct provided the feed rate is sufficient to avoid significant methanol depletion over the length of the channel. In the experiments described in the next section, the maximum total consumption of methanol was less than 3% of the feed, thus this approximation was well satisfied.

The combination of an imposed steady feed rate Q_s and oscillatory feed rate $Q(t)$ will result in a pressure gradient in the flow channel. The pressure gradient has been written as $\langle|\partial P/\partial x|\rangle$, since it represents the time-averaged magnitude of the pressure gradient; it is anticipated that time-dependent components will be averaged and may be out of phase with one another. For the time being, the model will be developed assuming $\langle|\partial P/\partial x|\rangle$ is known. Upon completing a description of the model, the methodology used to determine the pressure gradient in our experiments will be discussed.

In our model system, a pressure gradient is also present in the porous diffusion layer, but it produces a velocity which

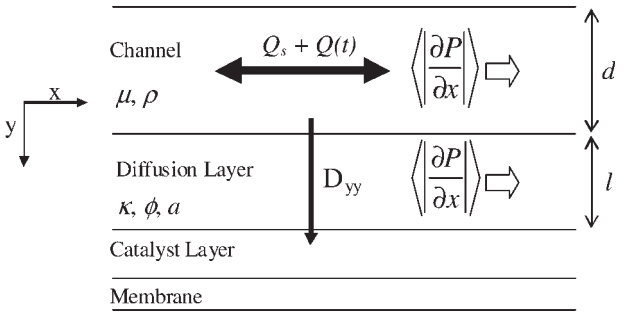

Figure 3. Simplified geometry of a DMFC anode used to develop a predictive model for the mass transport of methanol when an oscillatory flow $Q(t)$ is superimposed on a steady flow Q_s in the channel.

The fluid properties μ and ρ along with the geometric properties of the diffusion layer (κ, ϕ, a) are all considered to be constant. The time-averaged magnitude of the pressure gradient is the same in both the channel and the diffusion layer.

is smaller than the velocity in the channel by several orders of magnitude due to the small length scales of the pores. For unidirectional flow, the same $\langle|\partial P/\partial x|\rangle$ in the channel is also distributed throughout the porous diffusion layer, and thus the velocity in the diffusion layer can be estimated from Darcy's law:

$$U_{\mathrm{dl}} = -\frac{\kappa}{\mu}\left\langle\left|\frac{\partial P}{\partial x}\right|\right\rangle, \tag{1}$$

where κ is the permeability of the porous diffusion layer. In general, the permeability of a porous medium is often anisotropic. For the diffusion layers used in this study κ has been reported by the manufacturers only in the thin (transverse) direction. Assuming the medium is approximately isotropic, however, we may use these reported permeabilities to calculate the tangential velocity U_{dl} via Eq. 1 once the pressure gradient is known.

If the flow within the open volume of the porous diffusion layer was steady, the convective-diffusive behavior of methanol could be predicted using a steady flow model for a random fibrous porous medium such as that of Koch and Brady.[28] Provided the amplitude of the oscillatory flow is sufficiently large that memory is lost during each half-period of oscillation, it should also apply for oscillatory flows. This occurs if the condition $U_{\mathrm{dl}}/\omega a \gg 1$ is satisfied. In the majority of our experiments, $U_{\mathrm{dl}}/\omega a \geq 10$; consequently, it is assumed that the theory of Koch and Brady will be valid for oscillatory flow as well.

The Koch and Brady model calculates the effective diffusivity as a function of the flow regime present in the porous medium. The flow regime is determined by two related dimensionless quantities: the Peclet number (Pe) and the screening length Peclet number (Pe_{sc}), which are defined as

$$Pe = \frac{U_{\mathrm{dl}} a}{D_{\mathrm{o}}}; \quad Pe_{\mathrm{sc}} = \frac{U_{\mathrm{dl}} \kappa^{(1/2)}}{D_{\mathrm{o}}}, \tag{2}$$

where D_{o} is the molecular diffusion coefficient of the solute and a is the radius of the fibers in the porous diffusion layer.

Table 1. Reported and Calculated Permeabilities of the Diffusion Layers Used in Experimentation

Diffusion Layer	ϕ	κ (cm^2)	κ_e (cm^2)	η	λ
ELAT carbon cloth LT 1200-W	0.30	4.90×10^{-9}	2.18×10^{-8}	0.929	0.822
Toray carbon paper TGP-H-030	0.20	1.05×10^{-7}	1.05×10^{-7}	0.917	0.269
Toray carbon paper TGP-H-060	0.22	8.01×10^{-8}	8.49×10^{-8}	0.915	0.280

The fiber radius a was determined to be 4 μm for all three layers.

Koch and Brady also present an implicit method for estimating the permeability for fibrous porous media, which was originally derived by Speilman and Goren.[29] For the isotropic case,

$$\frac{1}{\kappa_e} = -\frac{\phi}{\pi a^2 \mu}\left[\frac{2}{3}f_\perp + \frac{1}{3}f_\parallel\right] + O\left[\frac{\phi}{a^2\left(\ln\left(\frac{1}{\phi}\right)\right)^2}\right], \quad (3)$$

where

$$f_\perp = -4\pi\mu\left[a\kappa_e^{-1/2}\frac{K_1\left(a\kappa_e^{-1/2}\right)}{K_0\left(a\kappa_e^{-1/2}\right)} + \frac{1}{2}a^2\kappa_e^{-1}\right],$$

$$f_\parallel = -2\pi\mu a\kappa_e^{-1/2}\frac{K_1\left(a\kappa_e^{-1/2}\right)}{K_0\left(a\kappa_e^{-1/2}\right)},$$

and κ_e is the estimated permeability of the porous medium, ϕ is the solid volume fraction of the fibers in the medium, and $K_0(x)$ and $K_1(x)$ are the modified Bessel functions of order zero and one. Values of κ and κ_e are presented in Table 1 along with additional geometric information on the diffusion layers used in the experiments. For the carbon fiber papers, the agreement between κ and κ_e is excellent, but the permeability of the carbon cloth is overestimated by a factor of four. The isotropic calculation of Eq. 3 should be accurate for the carbon fiber papers given their high porosities and random fiber orientations (Figure 4a). The carbon cloth, however, is a woven material composed of aligned bundles of fibers which overlap one another and the permeability is likely to be anisotropic. More significantly, however, examination of SEM images of the carbon cloth (Figure 4b) shows that much of the open area is obstructed by particulate material, decreasing the expected permeability. Thus, in our analysis, the measured permeabilities κ were employed for all diffusion layers.

Koch and Brady determined the effective diffusivity in the limit of low ϕ for several different flow regimes defined by Pe and Pe_{sc}. In this case, the diffusivity in the direction transverse to the flow (*i.e.* the y direction) is the value of interest. For $Pe \equiv 0$ and fibers which do not interact with the solute this diffusivity is given as

$$D_{yy} = \left(\frac{1}{1-\phi} - \frac{5}{3}\phi\right)D_o. \quad (4)$$

The other asymptote for the transverse diffusivity, described by the criteria $Pe \gg 1$ and $Pe_{sc} \gg 1$, is given as:

$$D_{yy} = \left(\frac{9}{6400}\pi^3\frac{a}{\kappa^{1/2}\phi}Pe\right)D_o, \quad (5)$$

which is purely mechanical dispersion due to the stochastic nature of the porous medium. A series of intermediate flow regimes are also described by Koch and Brady, but as an approximation the two asymptotes in Eqs. 4 and 5 are combined into the following

$$D_{yy} = (\eta + \lambda Pe)D_o, \quad (6)$$

where

$$\eta = \left(\frac{1}{1-\phi} - \frac{5}{3}\phi\right),$$

$$\lambda = \left(\frac{9}{6400}\pi^3\frac{1}{\kappa^{1/2}\phi}\right),$$

and the values of η and λ for each diffusion layer are given in Table 1. This simplification of the full theory captures the exact behavior of D_{yy} to within 10% over the entire range of Pe.

Predicting the transverse dispersivity D_{yy} is essential to development of a DMFC performance model because it is well known that the limiting current density i_{lim} is proportional to

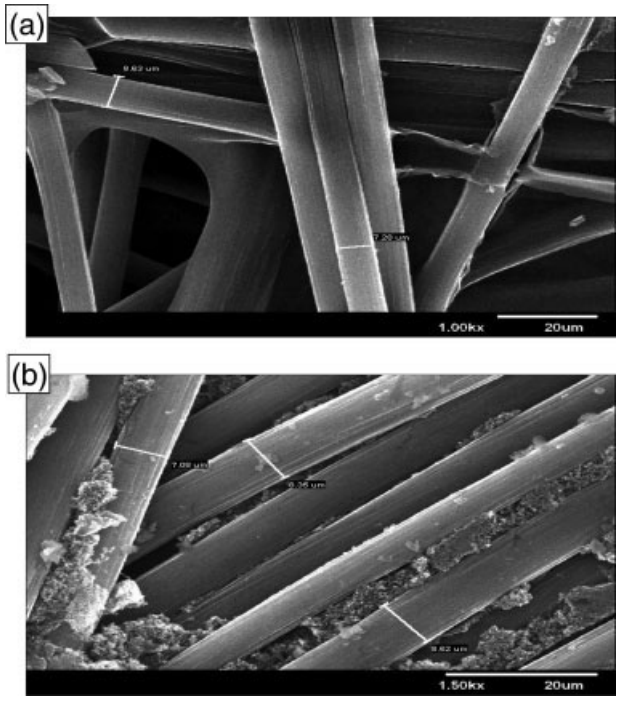

Figure 4. Scanning electron microscope images of (a) Toray carbon paper TGP-H-060 and (b) E-TEK ELAT carbon cloth.

An image of Toray carbon paper TGP-H-030 was not included, as its microstructure is very similar to that of the other carbon paper.

a total mass transfer coefficient k_{tot} which is a complex function of the geometry of the DMFC anode and the operating conditions.[4,14,30,31] In accordance with this observation, the following simple model is proposed:

$$\frac{1}{i_{lim}} = \frac{C}{k_{tot}} = C\left(\frac{1}{k_o} + \sum_{i=1}^{n} \frac{1}{k_i^{eff}}\right), \quad (7)$$

where C is a constant of proportionality, k_i^{eff} is the effective mass transfer coefficient in diffusion layer i, n is the number of different diffusion layers in the fuel cell anode, and k_o is the sum of the mass transfer limitations from the other components or mechanisms in the system. This model is equivalent to considering the anode as a series of mass transport resistances, of which the diffusion layer is one part, and is capable of handling composite layers such as those used in these experiments. Isolating k_i^{eff} from the other resistances in the system permits use of Eq. 6 to estimate transverse mass transport in the following manner:

$$k_i^{eff} = \frac{\delta(1-\phi_i)D_{yy,i}}{l_i} \approx \frac{\delta(1-\phi_i)D_o\eta_i}{l_i}(1+\lambda'_i Pe), \quad (8)$$

where l_i is the thickness of porous diffusion layer i, δ is the open area ratio, and $(1-\phi_i)$ adjusts for the void fraction of diffusion layer i. Note that the constant $\lambda'_i = \lambda_i/\eta_i$. Combining Eqs. 7 and 8 yields the expression

$$\frac{1}{i_{lim}} = C' + \sum_{i=1}^{n} \frac{C_i}{1+\lambda'_i Pe} \quad (9)$$

where the constants $C' = C/k_o$ and each C_i can be determined empirically. The limiting current density should thus vary between two asymptotes: a $Pe \ll 1$ limit where convective mass transport enhancement is absent (*i.e.* $C' + \Sigma C_i$) and a $Pe \gg 1$ limit where diffusional limitations in the porous diffusion layer are eliminated (*i.e.* C'). The transition between these limits, however, may be predicted without further adjustable parameters.

A modification of Eq. 9 can be made which reduces the number of empirically determined constants to one. Though k_o is an unknown combination of all the mass transport coefficients in the system besides the diffusion layer, it can be estimated from the experimental asymptote C'. The constant C is determined by a methanol flux balance to be $(6Fc_b)^{-1}$, where F is Faraday's constant and c_b is the concentration of methanol in the bulk. In practice, the conversion of methanol is quite small; therefore, the approximation $c_b \approx c_f$ (the feed concentration) is used. The model for the limiting current density then becomes

$$\frac{1}{i_{lim}} = \frac{1}{6Fc_f k_o} + \sum_{i=1}^{n} \frac{C_i^*}{1+\lambda'_i Pe}, \quad (10)$$

where

$$C_i^* = \frac{l_i}{6Fc_f\delta(1-\phi_i)\eta_i D_o},$$

and k_0 can be estimated from the $Pe \gg 1$ asymptote. It now remains only to determine $\langle|\partial P/\partial x|\rangle$ for oscillatory flow in the anode channel.

Oscillatory flow in the anode channel

To determine the pressure gradient, the detailed anode flow plate geometry must be considered. The geometry used in our experiments is depicted in Figure 5. It consists of three square parallel channels of width w, measured by a caliper to be 0.081 cm, and depth d. The channels have a length of 1.97 cm before expanding into flow reversal sections which are deeper (d_{fr}= 0.162 cm) and wider (w_{fr} = 0.162 cm). It was expected that the actual channel depth would deviate from its nominal depth when the DMFC was sealed because there is evidence which suggests that compressing the components of a fuel cell distorts the structure of the diffusion layer and causes it to occupy a fraction of the open area of the channel.[32]

Since the actual channel depth is not directly measurable when the DMFC is fully assembled and sealed, it was determined indirectly from measurement of the pressure drop-flow rate relationship. A series of experiments was performed where a known static head of fluid was applied to the assembled and sealed DMFC and the resulting flow rate in the DMFC was measured. This was done for all three diffusion layers and using fluids of two different viscosities: water and a solution of glycerin and water (90% glycerin by weight). The results of the measurements are presented in Figure 6.

For laminar flow at low Reynolds number the ratio of the pressure drop in the flow reversal section to that in the channels is approximately given by

$$\frac{\Delta P_{fr}}{\Delta P_{ch}} = \left(\frac{QL_{fr}}{2w_{fr}d_{fr}^3}\right) \times \left(\frac{QL_{ch}}{3wd^3}\right)^{-1} \approx 0.02, \quad (11)$$

where Q is the flow rate, ΔP_{fr} and L_{fr} are the pressure drop and length of the flow reversal sections, respectively, and ΔP_{ch} and L_{ch} are the pressure drop and length of the channel sections, respectively. The ratio in Eq. 11 is much less than

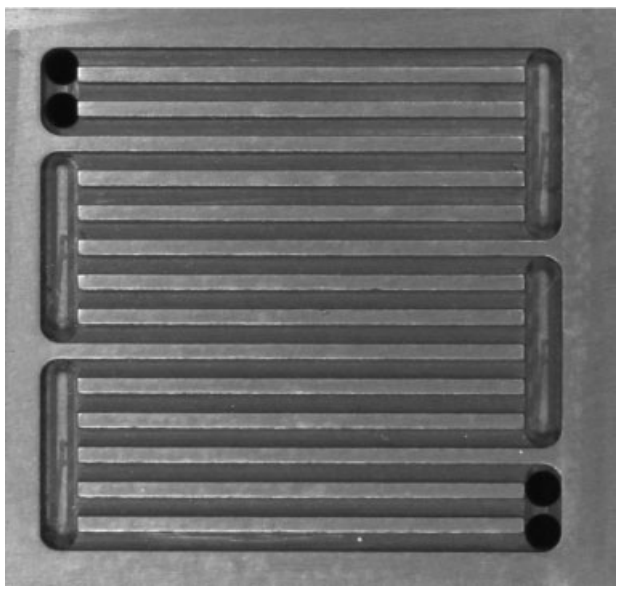

Figure 5. Graphite anode flow plate used in DMFC experiments.

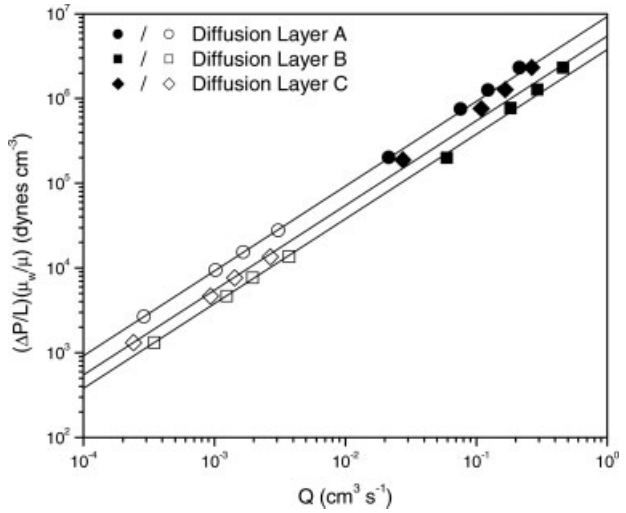

Figure 6. The relationship between pressure drop and flow rate, where the pressure drop is normalized by the ratio of the viscosity of water to the viscosity of the solution μ_w/μ, for the DMFC anode.

Experiments were performed at ambient temperature with the three diffusion layers used in experimentation. The fluids used were water (closed symbols) and 90 wt % glycerin/10 wt % water (open symbols). Lines of slope = 1 are provided as a reference.

one for our system, principally due to the greater depth of the flow reversal regions. Since this is the case, all sources of pressure loss are considered negligible compared to the pressure loss in the channels.

If the pressure drop is solely distributed along the anode channel length and the interface between the flow channel and the diffusion layer is assumed to act as a rigid wall, the velocity has a well-known analytical solution[33] which is a function of the unknown aspect ratio $\gamma = d/w$. Upon integrating the velocity to determine the flow rate, the following expression is obtained:

$$Q = \frac{w^4 \Delta P}{\mu L}\left(\sum_{n=1}^{\infty} -\frac{8\sin^2(\lambda_n)}{\lambda_n^5}\tanh(\lambda_n\gamma) + \frac{4}{3}\gamma\right), \qquad (12)$$

where the discrete eigenvalues $\lambda_n = \pi(n - 1/2)$. The expression in Eq. 12 can be used in conjunction with the relationship between Q and $\Delta P/L$ to solve for γ. The corresponding values of d are given in Table 2. The values of d calculated using this method demonstrate, somewhat surprisingly, that the diffusion layer occupies between 40 and 50% of the nominal anode channel depth.

Once the actual channel depth was known, the behavior of oscillatory flow in the anode flow plate was examined. The maximum amplitude of the velocity due to the fluid oscillations can be written as $U_{max} = \Delta V\omega/A_{ch}$, where the total cross-sectional area of the anode flow channels (three channels in parallel) is $A_{ch} = 3wd$. To characterize the oscillatory flow in the anode channels, a laminar-turbulent transition criterion which summarizes a large body of previous experimental work[34] is used. The transition criterion, in terms of the critical values (subscript c) of the relevant dimensionless parameters, is written as

$$Re_{max,c} \approx 400 Re_{\omega,c}^{1/2}, \qquad (13)$$

where $Re_{max} = U_{max}d_h/v$, $Re_\omega = \omega d_h^2/v$, and v is the kinematic viscosity of the fluid. The correlation given in Eq. 13 was developed for tubes and uses the hydraulic diameter d_h as the length scale. The anode channel is a rectangular duct and the hydraulic diameter is easily calculated. Values of d_h are given in Table 2. Since all geometric parameters are known, the criterion of Eq. 13 can be compared against values of Re_{max} and Re_w from the oscillatory flow experiments. The result of this analysis is presented in Figure 7. It is interesting to note that the majority of the oscillatory flow experiments were in the turbulent regime; it was necessary to reach the turbulent regime before pressure gradients large enough to induce significant mass transfer enhancement were achieved.

Table 2. Composition of the Diffusion Layers Used in DMFC Experiments

DL	Component 1	l_1 (cm)	Component 2	l_2 (cm)	d (cm)	d_h (cm)
A	ELAT cloth	0.027	–	–	0.046	0.059
B	ELAT cloth	0.027	TGP-H-030 paper	0.011	0.050	0.062
C	ELAT cloth	0.027	TGP-H-060 paper	0.019	0.043	0.056

The channel depth d and hydraulic diameter d_h were dependent on the diffusion layer composition.

Determination of the pressure gradient

For laminar flow, given that the pressure gradient has the form $G_o\sin(\omega t)$, the analytical solution for a channel is well known.[35] The solution can be written in dimensionless form as

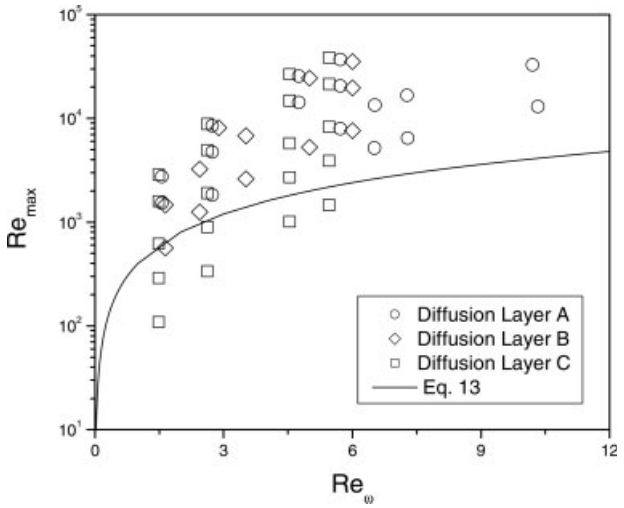

Figure 7. Operating conditions of the oscillatory experiments in this study compared to the laminar-turbulent transition criterion for oscillatory flow predicted by Eq. 13.

$$u^* = \Im\left\{\frac{\exp\left(it^*\right)}{Re_\omega^{*2}}\left[1 - \frac{\cosh\left(\frac{Re_\omega^* y^*}{i^{1/2}}\right)}{\cosh\left(\frac{Re_\omega^*}{i^{1/2}}\right)}\right]\right\} \tag{14}$$

where $u^* = (4u\mu)/(G_o d^2)$, $y^* = 2y/d$, $t^* = \omega t$, and $Re_\omega^* = Re_\omega(d^2/4d_h^2)$. This relationship can be expanded, integrated in space and time, and rearranged to solve for the time-averaged magnitude of the pressure gradient:

$$G_o = \frac{2\omega\Delta V\mu}{3wd^3} \times \left[\left(\frac{2}{Re_\omega^{*2}}\right)\left(1 - \frac{\left(\sin(\sqrt{2}Re_\omega^*) + \sinh(\sqrt{2}Re_\omega^*)\right)}{\sqrt{2}Re_\omega^*(\cos(\sqrt{2}Re_{*,\omega})) + \cosh(\sqrt{2}Re_\omega^*)}\right)\right]^{-1} \tag{15}$$

The value of G_0 calculated by Eq. 15 is equivalent to $\langle|\partial P/\partial x|\rangle$ and was used in Eq. 1 to determine the velocity in the porous diffusion layer for all laminar oscillatory flow experiments in the DMFC.

For the more important turbulent flow case, obtaining the pressure gradient is decidedly more challenging. For fully developed turbulent flow in a tube, the following unsteady momentum equation applies:

$$\frac{\partial P}{\partial x} = \rho\frac{\partial u}{\partial t} + \frac{4\tau_w}{R} \tag{16}$$

where τ_w is the wall shear stress and R is the tube radius. The first term is due to the acceleration and deceleration of the fluid, and can be calculated using the reasonable assumption that the spatially averaged velocity has the form $u = U_o\sin(\omega t)$. The second term is more difficult to calculate. If the flow was steady, τ_w can be determined using a friction coefficient f. In the oscillatory case, this is complicated by the scarcity of available correlations for fully turbulent oscillatory flow in a channel. However, similarities between the flow regimes of oscillatory turbulence and steady turbulence, including agreement between the Blasius correlation for steady turbulent flow and measurement of wall-friction velocities in oscillatory turbulent flow have been observed.[36] Therefore, the approach taken in this work is to estimate the oscillatory friction coefficient using an available correlation for steady turbulent flow. To calculate the friction coefficient, Re_{max} is not the appropriate dimensionless quantity; instead a Reynolds number is defined which accounts for the time-average of the flow:

$$\langle \mathrm{Re}\rangle = \frac{\langle U\rangle d}{v}, \tag{17}$$

where

$$\langle U\rangle = \frac{\Delta V}{3wd}\frac{\omega}{\pi}$$

that is, $\langle U\rangle$ is the time-averaged velocity. The maximum experimental value of $\langle \mathrm{Re}\rangle$ approached 10^4.

Upon expansion of the terms in Eq. 16, the approximate expression for the turbulent oscillatory pressure gradient becomes

$$\frac{\partial P}{\partial x} \approx -\rho\omega U_o\cos(\omega t) - 2f\frac{\rho U_o^2}{d}\sin(\omega t), \tag{18}$$

where the amplitude of the velocity $U_o = (\pi/2)\langle U\rangle$. The friction coefficient depends on the roughness of the walls and $\langle \mathrm{Re}\rangle$. In this case, the bottom wall of the channel is a layer composed of carbon fibers, many of which are likely protruding into the flow area. Assuming these protrusions are on the order of the pore radii, an available correlation for f[37] can be used

$$\frac{1}{f^{1/2}} = -4\log\left[\frac{0.27\varepsilon}{d_h} + \left(\frac{7}{\langle \mathrm{Re}\rangle}\right)^{0.9}\right], \tag{19}$$

where the absolute roughness ε was taken to be 1.0×10^{-3} cm. It should be noted that a few correlations for oscillatory turbulent flow in a pipe do exist,[38,39] but the parameter ranges in which they are valid coincide with only a few experiments performed in this work. In those selected experiments, the values of f calculated using the correlation of Ohmi et al. for oscillatory turbulent flow[38] were compared to the values of f obtained using Eq. 19; they were in good agreement, with a maximum deviation of 10%. The work of Ohmi et al. is based on a quasi-steady state approach for oscillatory turbulence that is appropriate when $\langle \mathrm{Re}\rangle \gg 700\sqrt{Re_\omega}$. This condition, in general, is satisfied by the oscillatory turbulent experiments of this work; based on this information it was surmised that using Eq. 19 to calculate f is a reasonable approach for this system.

The two contributions to the pressure gradient given in Eq. 18 are $\pi/2$ radians out of phase with one another. Because the Darcy's law flow in the porous diffusion layer is both laminar and low Reynolds number, the time-average magnitude of the pressure gradient is the quantity of interest. This is simply $2/\pi$ times the amplitude of the oscillatory pressure gradient, and this amplitude is the root mean square of the out of phase contributions in Eq. 18. Thus,

$$\left\langle\left|\frac{\partial P}{\partial x}\right|\right\rangle = \frac{2}{\pi}\left[(\rho\omega U_o)^2 + \left(2f\frac{\rho U_o^2}{d}\right)^2\right]^{1/2}, \tag{20}$$

which can be further simplified using the definition of:

$$\left\langle\left|\frac{\partial P}{\partial x}\right|\right\rangle = \frac{\rho\omega^2\Delta V}{3\pi wd}\left[1 + \left(\frac{f\Delta V}{3wd^2}\right)^2\right]^{1/2}. \tag{21}$$

For the parameter ranges of the experiments, the magnitude of $(f\Delta V/3wd^2)$ varied from 1.0 to 38.7. In the turbulent oscillatory experiments, therefore, the friction at the channel walls was the dominant contributor to the time-averaged turbulent pressure gradient.

To review, the estimate of the time-average magnitude of the pressure gradient given either by Eq. 15 or 20 depending on the flow regime in the anode channel was used in Eq. 1 to solve for the velocity in the porous diffusion layer. Since the oscillatory flow has sufficient amplitude to be considered steady, D_{yy} was computed using Eq. 6 for all the experiments. With this information, the models given by Eqs. 9 and 10 were used to predict the limiting current density and compared to experimentally observed values.

Experimental Method

Recent work[40] has indicated that high-throughput electrocatalyst screening systems are a good barometer of expected DMFC performance. To validate that the oscillatory technique had promise enough to warrant further study in a DMFC, preliminary experimentation was performed using the multiarray high-throughput electrocatalyst screening system NUV100P (Nuvant Systems, Crown Point, IN) with a Johnson-Matthey 50:50 Pt-Ru catalyst on carbon black. The diffusion layer was carbon paper TGP-H-060 (Toray Industries, Decatur, AL). A solution of 0.5 M CH_3OH in water was fed to the anode at 8 $cm^3\ min^{-1}$. Humidified H_2 at 60°C was fed to a common counter electrode at 180 $cm^3\ min^{-1}$. The cell temperature was held constant at 80°C. An oscillatory syringe pump with a manually variable stoke volume ($0.01\ cm^3 < \Delta V < 0.90\ cm^3$) and frequency ($1.32\ rad\ s^{-1} < \omega < 38.83\ rad\ s^{-1}$) was positioned in-line just after the methanol feed pump with a tee junction. First, a series of transient experiments were performed. The voltage was forced to be constant, the oscillatory pump was activated, and the response of the cell was measured. Second, linear sweep voltammetry (LSV) tests were performed, with a scan rate of 6 mV s^{-1} from 0.0 to 1.0 V vs. the dynamic hydrogen electrode.

All DMFC experimentation was performed in a single cell (ElectroChem, Woburn, MA) with an active area $A_e = 5\ cm^2$ (2.236 cm × 2.236 cm). The cell contained two gold-plated copper end plates, two graphite current collectors with the previously described flow field (Figure 5), and two Teflon gaskets sandwiched around the membrane electrode assembly (MEA). The cell was secured by eight bolts tightened to 6.2 N m with a torque wrench. The MEA used was a commercially available product from www.fuelcellstore.com (Boulder, CO). It consisted of a Nafion 117 membrane with 4.0 mg cm^{-2} Pt/Ru (1:1 atomic ratio) and 2.0 mg cm^{-2} Pt as the catalyst loadings on the anode and cathode, respectively. The diffusion layer (DL) on both the anode and cathode was composed of different composites of varying structure and thickness l_i. The three different composites used are summarized in Table 2.

Experiments were performed using a gas distribution system (Teledyne Medusa™ RD), an 890C methanol flow control unit (Scribner Associates, Southern Pines, NC), and an 890C-100W fuel cell test load (Scribner Associates). The three units were controlled and monitored by the software package Fuel Cell® for Windows (Scribner Associates). The gas distribution system was used to deliver humidified hydrogen at a cell temperature of 50°C and a flow rate of 100 $cm^3\ min^{-1}$ to pretreat the MEA. The hydrogen was delivered for a period of 10 h to both the anode and the cathode. After the MEA pretreatment, the anode and cathode inlets and outlets were connected to the 890C-MeOH flow control unit. The oscillatory syringe pump described previously was placed in-line with the anode feed using a tee junction. The majority of experiments were performed at a cell temperature of 70°C and ambient pressure. The anode feed solution was 1.0 mol L^{-1} methanol in distilled water, and the cathode feed was pure oxygen. The flow rates of the anode and cathode were 12 and 500 $cm^3\ min^{-1}$, respectively. The open circuit potential (OCP) was allowed to stabilize at these flow rates.

Performance measurements were made by scanning the voltage, controlled by the 890C-100W fuel cell test load and the accompanying software, at a rate of 5 s per data point from the OCP to zero. Before any measurements were taken with the oscillatory syringe pump in operation, the DMFC was heat treated by varying the cell temperature. During the heat treatment of the DMFC, the voltage scan was also reversed back to the OCP; no significant hysteresis was observed. After the heat treatment, the DMFC was returned to the cell temperature of interest (typically 70°C). A baseline voltage scan was performed, in which the anode feed rate had only a steady flow component. This was followed by a series of voltage scans with an oscillatory flow component superimposed upon the steady flow using the syringe pump. At a particular stroke volume, experiments were performed across the range of available frequencies. Each experiment was performed a minimum of twice to verify the observed behavior. This procedure was repeated at several other stroke volumes.

Results

As mentioned, initial experimentation was performed using the NUV100P. Since no cathode reaction was taking place, measurements taken in the NUV100P isolated the behavior of the anode. Though it does not perfectly mirror what occurs in a full cell DMFC since several of the factors affecting DMFC performance are coupled with one another, it does eliminate the possibility of mass transfer limitations being affected by activity at the cathode, as well as eliminating the effect of methanol crossover. Nonstandard behavior resulting from these experiments is certain to be solely due to changes in mass transport behavior in the anode flow field and porous diffusion layer.

A typical transient current density response is given in Figure 8. It is clear that inducing fluid oscillations has an appreciable effect on the current-voltage behavior of the anode. Three important characteristics of the anode's response when oscillatory flow is induced can be recognized from the experiment: the current density improves instantaneously, the improvement remains stable for as long as the oscillations are present, and it is reproducible (that is, improvements can be recovered again by reinstating the fluid oscillations).

The LSV tests, such as the series performed at a constant stroke volume in Figure 9, demonstrate the other important characteristic of the anode's response to oscillatory flow. There is no observed difference between steady and oscillatory flow experiments when the potential is below 0.6 V. At these potentials, the response of the anode is due to kinetics and membrane conductivity. At potentials above 0.6 V, the anode is limited by mass transport and there is significant improvement when oscillatory flow is present. The improvement increases with the oscillation frequency. At the highest frequencies, the power density improved by greater than 30% at high cell potentials.

The results from the NUV100P motivated further experimentation in the DMFC. A summary of the essential features of the DMFC experiments is presented in Figure 10. Each column in the figure corresponds to a different stroke volume, while each row corresponds to a different diffusion layer. Visual comparison of these graphs with one another

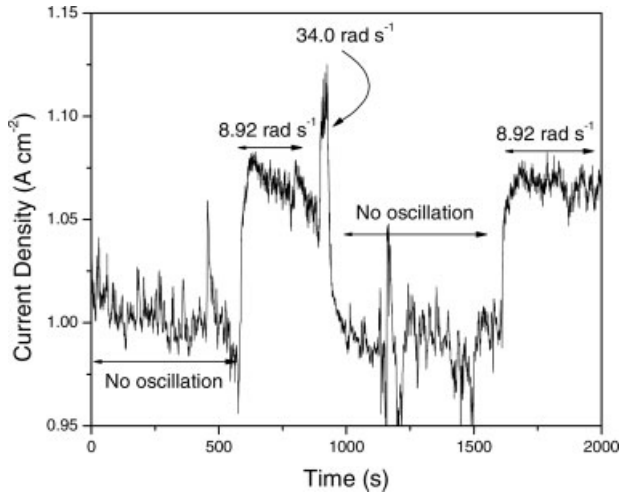

Figure 8. The transient response of a standard DMFC anode catalyst in the NUV100P to induced fluid oscillations.

The cell potential was held constant at 1.0 V vs. the dynamic hydrogen electrode, the cell temperature was 80°C, the steady feed rate was 8 cm^3 min^{-1}, and the stroke volume was 0.17 cm^3.

yields several qualitative observations concerning the mass transfer behavior of the DMFC when the anode is exposed to an oscillatory flow.

First, from a comparison of the polarization curves obtained when the anode feed was steady, it was observed that i_{lim} increased with decreasing diffusion layer thickness. Since all experimentation was performed at the same cell temperature, this is to be expected if the limiting current is indeed proportional to a total mass transfer coefficient. Despite the complexity of the geometry and flow field, decreasing the distance over which a solute must diffuse will increase the flux of solute through the medium, provided the driving force remains the same.

Second, the polarization curves distinctly demonstrate that the oscillatory flow improves mass transport in the DMFC anode once a critical amplitude is achieved. There is no observed difference between steady flow operation and oscillatory flow operation in either the kinetically limited region or the ohmic region of the polarization curves. Deviation from steady flow experiments occurred only at high current densities when saturation of the current density had begun (*i.e.* region 3 in Figure 2). Thus, fluid oscillations did not affect membrane resistance or reaction kinetics in the DMFC, as would be expected.

Third, experiments performed with Diffusion Layer A (see Figures 10a,d,g) illustrate that the potential for enhancement in the mass transfer limiting region is only accessible when the amplitude of the oscillations are large; that is, the combination of ΔV and ω results in large values of U_0. The requirement that the value of U_0 be large is also observed to a lesser extent in the experiments using Diffusion Layer B (Figures 10c,f,i). In the case of Diffusion Layer C (Figures 10b,e,h), enhancement in i_{lim} is present even at smaller values of U_0; this is not unreasonable because layer C, which is thicker, had a greater degree of mass transfer limitation in the absence of oscillations.

Fourth, the magnitude of the improvement in experimental values of i_{lim} suggest significant enhancement in mass transport. Typical improvements in limiting current density range from 50 to 80%. In a few cases the improvement is greater than 100%. This suggests that the total mass transfer coefficient was improved by as much as a factor of two.

Finally, enhancement in peak power density was also observed during experimentation. Such improvement was possible only in cases where the performance decay characteristic of mass transfer limitations occurred before the peak value was reached in the steady flow experiment. In these experiments, one example of which is Figure 10c, the peak power density was increased up to a maximum of 30%.

Additional experiments were performed in the DMFC using Diffusion Layer A and a syringe pump capable of accessing frequencies up to 251 rad s^{-1}. Investigation in this parameter range was motivated by the results presented in Figures 10a,d,g. It was desirable to see if DMFC performance with layer A could be enhanced more significantly than was possible using the initial frequency range. The results of this investigation appear in Figure 11. Despite the reduced cell temperature, it is evident from the experiments that mass transport can be enhanced significantly in the cloth diffusion layer if the frequency is increased.

There are a few items to note from experimentation in the higher frequency range. First, the stroke volume that was used is the same as in Figure 10a. This is significant because a diffusion layer which appeared to have a resistance that negated the effect of oscillatory flow did in fact have capacity for mass transport enhancement when higher frequencies were used. Second, we observed the instantaneous nature of the transition between oscillatory flow performance and steady flow performance in the experiment where ω = 94.6 rad s^{-1}. When the oscillations were discontinued during the voltage scan, the current density quickly reverted back to align with the behavior observed during steady flow operation. Lastly, the experiments suggest that there is a trade-off

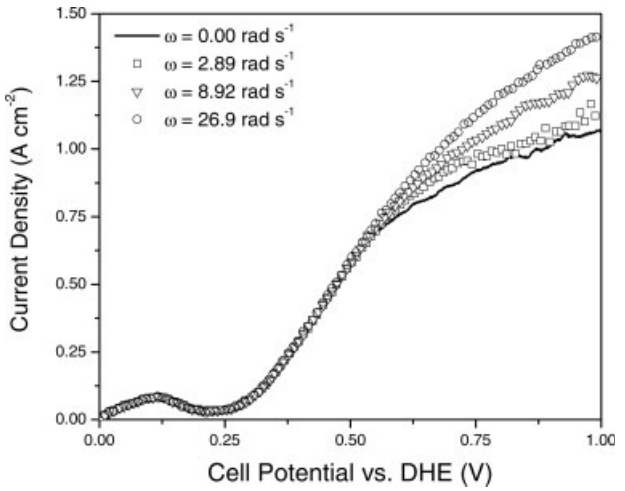

Figure 9. Current density response of a standard DMFC anode catalyst in the NUV100P to a LSV test.

The cell temperature was 80°C, the steady feed rate was 8 cm^3 min^{-1}, and the stroke volume was 0.44 cm^3.

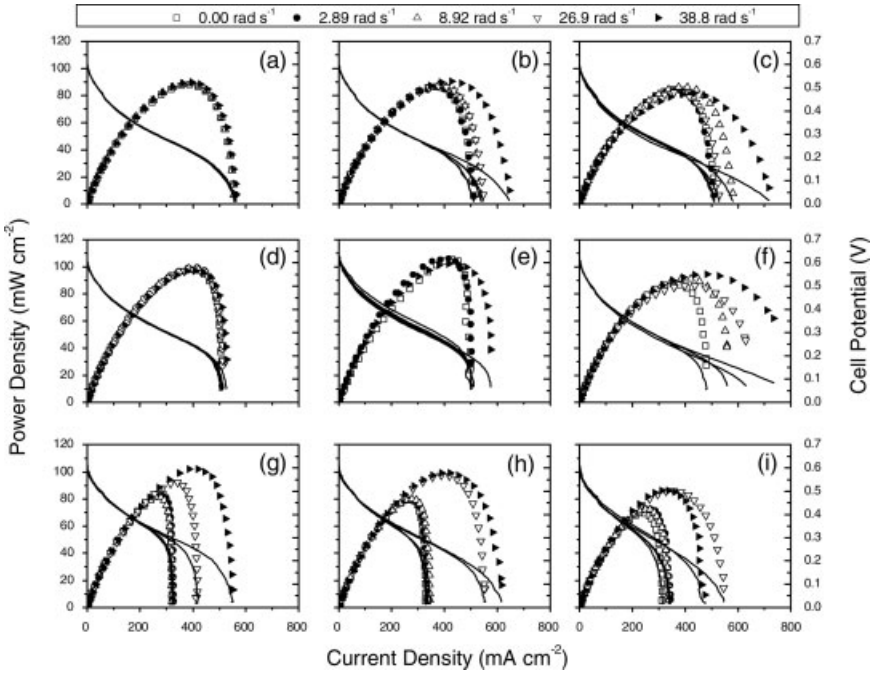

Figure 10. DMFC polarization curves obtained at 70°C for: (a–c) Diffusion Layer A, (d–f) Diffusion Layer B, (g–i) Diffusion Layer C.

The stroke volumes were 0.17, 0.44, and 0.79 cm^3 for the first, second, and third columns, respectively. The anode feed rate was 12 cm^3 min^{-1} and the cathode feed rate was 500 cm^3 min^{-1}.

between frequency (or more precisely, U_0) and performance, in the sense that above a frequency threshold ($\sim$125 rad s^{-1} in this case) only minimal gains in i_{lim} were observed. This is not surprising because other mass transfer resistances would ultimately dominate the overall resistance.

Discussion

Experimental observations show that inducing oscillatory flow in the anode of a DMFC enhances performance at high current densities. At some operating conditions, the enhanced performance not only manifested as an appreciable gain in limiting current density, but also larger peak power densities. This enhancement was due to a significant decrease in overall mass transfer limitations. As previously mentioned, mass transfer limitations have traditionally been attributed to two mechanisms: physical blockage of the diffusion layer pores by CO_2 gas and the inability of the solutes (in particular, methanol) to diffuse quickly enough to the catalyst surface.

In previous work where evolved CO_2 gas was directly observed to correspond with reduced performance at high current densities,[7] the steady flow rates to the anode were low (that is, <8 cm3 min^{-1}) for a cell of similar size. In those experiments, nearly all CO_2 bubbles were removed at steady flow rates >4 cm^3 min^{-1} at the expense of reduced performance. It has also been demonstrated that performance can be recovered by significantly increasing the flow rate if the anode feed is preheated.[41,42] In our experiments, however, the anode feed was at ambient temperature and increasing the flow rate negatively affected the performance by decreasing the overall cell temperature, as shown in Figure 12. Increasing the flow rate from 12 to 50 cm^3 min^{-1} did not affect the limiting current density; the peak power density, however, was decreased significantly. Increasing the flow rate by additional factor of 5 to 250 cm^3 min^{-1} further decreased the peak power output. The slight increase in i_{lim} at this flow rate is not surprising: its magnitude is compara-

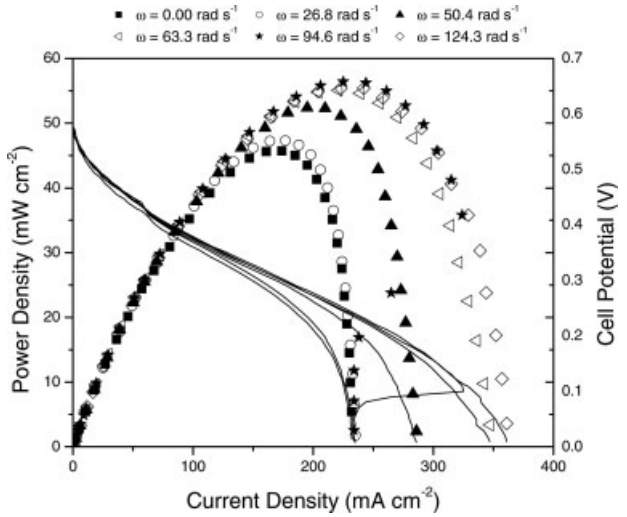

Figure 11. DMFC polarization curves obtained at 50°C for ΔV = 0.17 cm^3 using Diffusion Layer A.

The anode feed rate was 12 cm^3 min^{-1} and the cathode feed rate was 500 cm^3 min^{-1}.

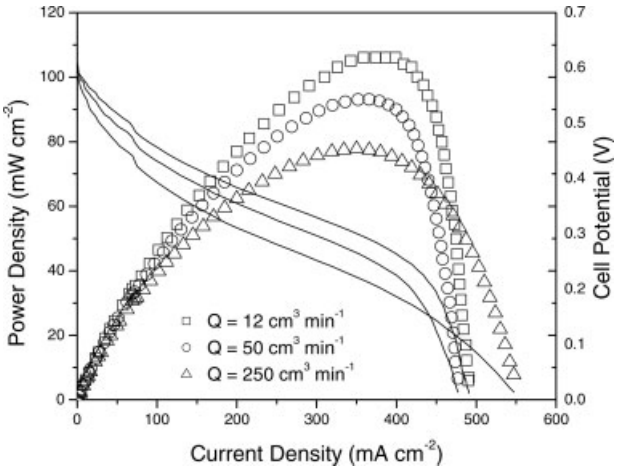

Figure 12. The effect of increasing the steady feed rate on DMFC performance.

The cell temperature was 70°C and the cathode feed rate was 500 cm^3 min^{-1} using Diffusion Layer A.

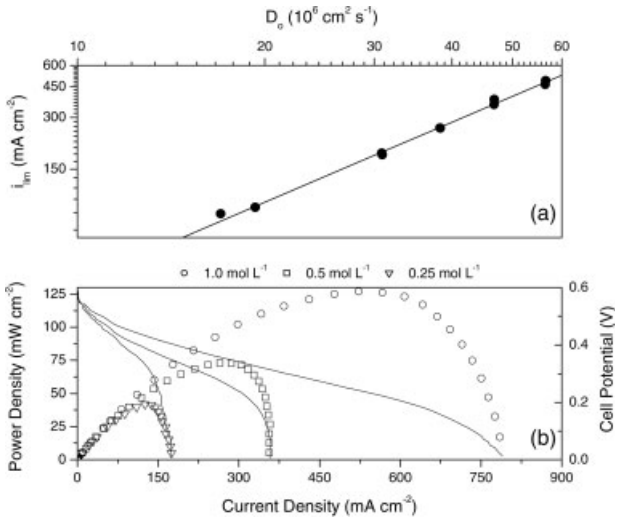

Figure 13. (a) The relationship of the limiting current to the molecular diffusion coefficient of methanol in the DMFC; (b) DMFC polarization curves obtained at 70°C and the same conditions as (a), with the exception of the methanol feed concentration.

For (a), the experiments were performed using an anode feed rate of 12 cm^3 min^{-1}, a cathode feed rate of 500 cm^3 min^{-1}, and Diffusion Layer C. The cell temperatures used were 25, 30, 50, 60, 70, and 80°C. The solid line is provided as a reference; it is a line of slope = 3/2. Note that the limiting current density increases by a factor of two as the methanol feed concentration is increased by two.

ble to that of the oscillatory flow where mass transport enhancement was first observed in Figure 10. Therefore, an anode flow rate of 12 cm^3 min^{-1} appeared to be sufficient to sweep out a large portion of the CO_2 bubbles, but not so large as to significantly cool the cell. All experiments depicted in Figure 10 were performed at this flow rate.

The dependence of the limiting current density on the molecular diffusion coefficient of methanol is presented in Figure 13a. D_0 was varied by changing the cell temperature from room temperature to 80°C. The cell temperature also influences other variables in the DMFC, such as reaction rate, membrane properties, and liquid–gas equilibria, making it difficult to isolate the effect that the diffusion of methanol has on limiting current. For the temperature range considered in Figure 13a, $i_{\lim} \sim D_o^{3/2}$. The limiting current density clearly has a dependence on the diffusion rate of methanol; that the relationship is not exactly linear is probably due to the temperature dependence of other mechanisms in the DMFC. The issue can be further resolved if the methanol concentration in the feed is varied, as it is in Figure 13b. When the methanol concentration is reduced by two, $i_{\lim}$ is also reduced by a factor of two. This proportionality would not be expected if carbon dioxide was playing a significant role in the mass transport behavior at high current densities. It appears reasonable, therefore, to conclude that the dominant mass transfer resistance when the DMFC is operated at high flow rates and low methanol feed concentrations is the diffusion of methanol.

We now apply our simplified mass transfer model to the oscillatory flow experiments. The model given by Eq. 9 has two or three empirical constants depending on the diffusion layer. It is presented along with experimental data in Figure 14. As Figure 14 shows, the model is in good quantitative agreement with observed limiting current densities. The transition between the two asymptotic regions ($Pe \rightarrow 0$ and $Pe \rightarrow \infty$) is captured quite well. The model isolates the mass transfer resistance of the diffusion layer and is a function of Pe only. It is significant that the improvements in $i_{\lim}$ observed experimentally rapidly increase when $Pe \geq 1$; this is consistent with the assumption that the diffusion of methanol was convectively enhanced by the fluid oscillations.

The modified model of Eq. 10 was in reasonable agreement with the experimental data, but it overestimated the mass transfer resistance of the diffusion layers. As Table 3

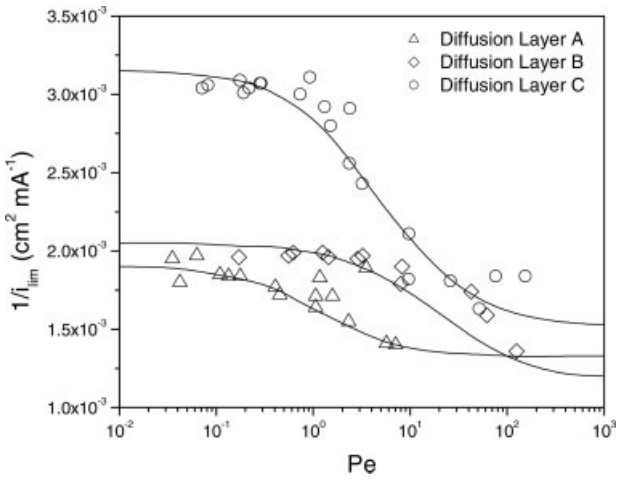

Figure 14. Model (solid lines) described by Eq. 9 compared to limiting current densities measured in DMFC experiments (open symbols) as a function of *Pe*.

Table 3. Total Mass Transfer Coefficients of the Diffusion Layers at the Two Extrema of the Experiments

DL	k_{tot}^{∞} (cm s^{-1})	k_{tot}^{0} (cm s^{-1})	Pred. k_{tot}^{0} (cm s^{-1})
A	1.31×10^{-3}	9.09×10^{-4}	4.54×10^{-4}
B	1.51×10^{-3}	8.43×10^{-4}	3.82×10^{-4}
C	1.17×10^{-3}	5.48×10^{-4}	3.11×10^{-4}

The superscript refers to the corresponding *Pe* asymptote. The predicted value as $Pe \rightarrow 0$ is calculated using Eq. 10. Refer to Table 2 for the compositions of each layer.

shows, the values of k_{tot} as $Pe \rightarrow 0$ calculated using Eq. 10 are smaller than the values of k_{tot} from the experimental data by 45 to 55%. The smaller values of k_{tot} are more than likely a result of the simplicity of the model, which only considers methanol transport in the y direction. It ignores the potential for methanol to diffuse under the ribs of the anode channel, thereby reacting at more catalyst sites, and the influence of carbon dioxide gas. Qualitatively, however, the mass transfer behavior of the DMFC—in particular the transition between the two *Pe* asymptotes—was captured by Eq. 10 for all three diffusion layers.

Inducing oscillatory flow also improved the peak power density of the cell in some experiments. The technique will not be advantageous, however, if the power required to induce the oscillations eclipses the observed enhancements in power density. The mechanical power, neglecting losses, can be estimated as

$$\Psi \approx Q_o \Delta P, \tag{22}$$

where Ψ is the power, ΔP is the pressure difference over the length of the anode channel and Q_0 is the amplitude of the oscillatory volumetric flow rate. Eq. 22 represents the minimum power required to generate fluid oscillations independent of the methodology that is used. Improvements in the peak power density were observed for $\langle Re \rangle \geq 10^3$. Consequently, the flow was turbulent and the pressure contribution due to friction at the walls given by the second part of Eq. 18 was the dominant source of pressure loss. To simplify the analysis, the pressure gradient in the channel is assumed to be represented by the frictional source only, so Ψ can be written as

$$\Psi \approx Q_o \frac{\partial P}{\partial x} L = \frac{\Delta V \omega L}{2} \frac{2\rho f}{d} U_o^2 = \frac{1}{36} \frac{\rho f L}{w^2} \left(\frac{\omega \Delta V}{d} \right)^3, \tag{23}$$

where L is the total length of the channel in the anode flow plate. To signify that Eq. 23 is estimating the minimum power required to drive the oscillations, it will be recast as $\Psi_{min} = \Psi / A_e$, which is a power density. In this form it can be directly compared to measured power densities from the experiments. The ratio of the power density in an oscillatory experiment Ψ_{osc} normalized by the power density in the corresponding steady flow experiment Ψ_o is presented in Figure 15 against Ψ_{min}, which is also normalized by Ψ_o. The relationship $\Psi_{osc}/\Psi_o = 1 + \Psi_{min}/\Psi_o$ was added; it is the break even point at which the oscillatory flow produces more power than it requires. It is clear from examining Figure 15 that for the DMFC tested the energy dissipated in the fluid exceeded the gain in power output for nearly all conditions.

To use fluid oscillations to efficiently increase power output it is necessary to alter the properties of the diffusion layer, specifically reducing the pressure gradient required to achieve the Darcy's law flow which produces the mass transfer enhancement. For example, the relationship between pressure drop and the diffusion layer velocity is already known from Eq. 1, and using the limit of the isotropic permeability defined in Eq. 3 when ϕ is small,

$$U_{dl} \sim \frac{a^2 \ln(\phi^{-1})}{\phi \mu} \frac{\partial P}{\partial x}. \tag{24}$$

The scaling suggested in Eq. 24 can be combined with the definition of the Peclet number to yield

$$Pe \sim \frac{a^3 \ln(\phi^{-1})}{\phi \mu D_o} \frac{\partial P}{\partial x}, \tag{25}$$

which indicates that if a is doubled while the solid fraction ϕ remains the same, the pressure gradient required to produce the same *Pe* is reduced by a factor of 8.

The same type of analysis can be extended using the definition of power in Eq. 22, again assuming that the turbulent oscillatory pressure gradient is only due to friction. Darcy's law can be used to relate U_0 to U_{dl} along with the relationship of Eq. 24 to give the following:

$$U_o = \left(\frac{U_{dl} \mu d}{2\kappa f \rho} \right)^{1/2} \sim K \left(\frac{\partial P}{\partial x} \right)^{1/2}, \tag{26}$$

where K is a collection of geometric and fluid property constants. Combining Eq. 26 with the scaling given in Eq. 25 yields:

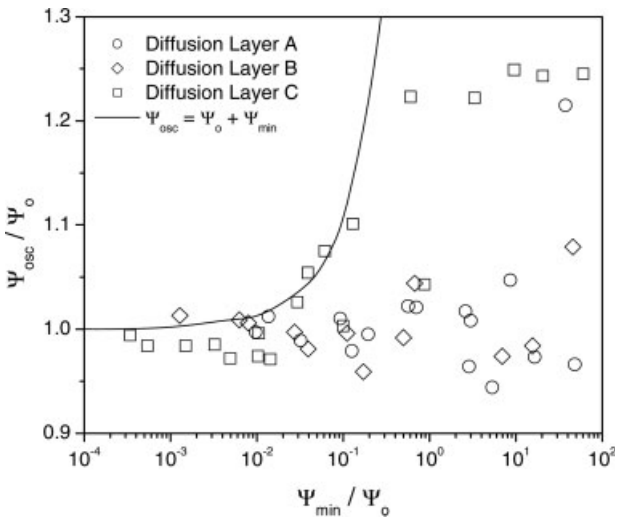

Figure 15. The peak power density in an oscillatory flow experiment Ψ_{osc} for the three diffusion layers plotted against the minimum power density required to induce the oscillatory flow Ψ_{min}.

Each quantity is normalized by the peak power density in the corresponding steady flow experiment Ψ_0. The power requirement break even point is represented by the solid line. Scatter in the data points is due to different means of generating oscillatory flow in the diffusion layer (e.g. ω or ΔV).

$$\Psi \sim \frac{Pe^{3/2}}{a^{9/2}}, \tag{27}$$

which suggests that increasing a by a factor of two will reduce the minimum power requirement to drive the fluid oscillations at fixed Pe by more than a factor of 20. This would have the effect of shifting the data points in Figure 15 to the left by a factor of 20, leading to efficient enhancement of the peak power density, at least for thicker diffusion layers.

Conclusions

An oscillatory flow was superimposed upon the steady feed of a methanol/water solution to the anode of a DMFC. It was demonstrated that performance improvements can be obtained using this technique, even without optimization of the system parameters; in particular, significant increases in the limiting current density (up to 100%) and peak power density (up to 30%) were observed. A mass transfer model was developed using an existing theory of dispersion in a fibrous porous medium to predict the observed limiting current densities as a function of the Peclet number in the diffusion layer of the anode. The steady flow condition (*i.e.* $U_{dl}/\omega a \gg 1$) was satisfied in these experiments, and the theoretical prediction was in good agreement with experiments performed using three different diffusion layers. The limiting current was found to increase rapidly as $Pe \geq 1$, which suggests that the diffusion of methanol is convectively enhanced in the direction transverse to the oscillatory flow. The primary mass transfer resistance in the DMFC anode at high current densities for the operating conditions of this study is the diffusion of methanol to the catalyst surface.

There are several ways in which an appropriately designed DMFC could take advantage of the results of this work. For example, it is not always desirable to operate at the high current densities where the technique is effective, for reasons of both catalyst utilization and gas removal. In such situations, oscillations in the anode feed are unnecessary. However, if a greater power output or a higher current density were required, fluid oscillations could be induced, leading to an instantaneous increase in accessible power densities and limiting currents.

A DMFC with an implemented oscillatory flow generation method could also take advantage of using a thicker diffusion layer, provided the diffusion layer has an open structure. A thicker diffusion layer would permit the use of higher methanol concentrations in the anode feed, and thus better performance at low current densities because the methanol crossover will be reduced. At high current densities, oscillatory flow would be used to eliminate the resistance of the diffusion layer by improving the mass transfer in the porous medium.

In regard to catalyst utilization, the DMFC is typically loaded with ≤ 4 mg cm^{-2} Pt:Ru at the anode. The DMFC is not optimized for high loadings as mass transfer limitations result in inefficient use of the catalyst. Reducing such limitations would improve catalyst utilization at high current densities.

Given the prohibitive power requirements which were presented in Figure 15, however, using oscillatory flow as a diagnostic tool is its most promising application. The present study has shown that if appropriate values of ΔV and ω are chosen, the oscillations will produce an enhancement in the mass transfer which is easily observable as an increase in limiting current density. It has also been observed that MEAs which are not kinetically active enough to reach the mass transport limitation regime are not affected by the oscillations and the polarization curve is unchanged. Generating oscillations would be a simple technique to determine if mass transport limitations do exist in a particular DMFC or for a particular MEA, and if they do, to estimate the relative magnitude of the limitations. Additionally, oscillatory flow could be used to permit other elements of the DMFC, such as anode kinetics or membrane transport, to be studied without the interference of mass transport limitations.

There are other design or operational variables which were unexplored in this experimental study, but will have effect on the mass transport behavior of methanol in the DMFC anode. Notably, neither the effect of the concentration of methanol in the anode feed nor the steady flow rate upon which the oscillatory flow is superimposed were studied. The effect of these variables and an optimization of the oscillatory technique and flow field geometry are left to future efforts. Regardless, this work has demonstrated that oscillatory flow enhances mass transport and has the potential to significantly improve performance in an appropriately designed DMFC.

Acknowledgments

This work was supported by the United States Army CECOM RDEC through Agreement No. DAAB07-03-3-K414. The authors would also like to thank Dr. Tim Hall for his assistance in obtaining the SEM images in Figure 4.

Literature Cited

1. Schultz T, Zhou S, Sundmacher K. Current status of and recent developments in the direct methanol fuel cell. *Chem Eng Technol.* 2001;24:1223–1233.
2. Aricò AS, Srinivasan S, Antonucci V. DMFCs: from fundamental aspects to technology development. *Fuel Cells.* 2001;1:133–161.
3. Heinzel A, Barrágan VM. A review of the state of the art of the methanol crossover in direct methanol fuel cells. *J Power Sources.* 1999;84:70–74.
4. Scott K, Taama WM, Kramer S, Argyropoulos P, Sundmacher K. Limiting current behaviour of the direct methanol fuel cell. *Electrochim Acta.* 1999;45:945–957.
5. Kulikovsky AA. Model of the flow with bubbles in the anode channel and performance of a direct methanol fuel cell. *Electrochem Commun.* 2005;7:237–243.
6. Lu GQ, Wang CY. Electrochemical and flow characterization of a direct methanol fuel cell. *J Power Sources.* 2004;134:33–40.
7. Yang H, Zhao TS, Ye Q. In situ visualization study of carbon dioxide gas bubble behavior in direct methanol fuel cell anode flow fields. *J Power Sources.* 2005;139:79–90.
8. Scott K, Taama WM, Argyropoulos P, Sundmacher K. The impact of mass transport and methanol crossover on the direct methanol fuel cell. *J Power Sources.* 1999;83:204–216.
9. Scott K, Argyropoulos P, Sundmacher K. A model for the liquid feed direct methanol fuel cell. *J Electroanal Chem.* 1999;477:97–110.
10. Nordlund J, Lindbergh G. A model for the porous direct methanol fuel cell anode. *J Electrochem Soc.* 2002;149:A1107–A1113.
11. Guo H, Ma C. Two-dimensional analytical model of a direct methanol fuel cell. *Electrochem Commun.* 2004;6:306–312.
12. Cruickshank J, Scott K. The degree and effect of methanol crossover in the direct methanol fuel cell. *J Power Sources.* 1998;70:40–47.

13. Ge J, Hongtan L. Experimental studies of a direct methanol fuel cell. *J Power Sources*. 2005;142:56–69.
14. Xu C, He YL, Zhao TS, Chen R, Ye Q. Analysis of mass transport of methanol at the anode of a direct methanol fuel cell. *J Electrochem Soc*. 2006;153:A1358–A1364.
15. Amphlett JC, Peppley BA, Halliop E, Sadiq A. The effect of anode flow characteristics and temperature on the performance of a direct methanol fuel cell. *J Power Sources*. 2001;96:204–213.
16. Yang H, Zhao TS. Effect of the anode flow field design on the performance of liquid feed direct methanol fuel cells. *Electrochim Acta*. 2005;50:3243–3252.
17. Xu C, Zhao TS. A new flow field design for polymer electrolyte-based fuel cells. *Electrochem Commun*. 2007;9:497–503.
18. Nordlund J, Roessler A, Lindbergh G. The influence of electrode morphology on the performance of a DMFC anode. *J Appl Electrochem*. 2002;32:259–265.
19. Oedegaard A, Hebling C, Schmitz A, Møller-Holst S, Tunold R. Influence of diffusion layer properties on low temperature DMFC. *J Power Sources*. 2004;127:187–196.
20. Xu C, Zhao TS, Ye Q. Effect of anode backing layer on the cell performance of a direct methanol fuel cell. *Electrochim Acta*. 2006;51:5524–5531.
21. Xie F, Chen C, Meng H, Shen PK. Effect of the anodic diffusion layer on the performance of liquid fuel cells. *Fuel Cells*. 2007;7: 319–322.
22. Zhang J, Yin GP, Lai QZ, Wang ZB, Cai KD, Liu P. The influence of anode gas diffusion layer on the performance of low-temperature DMFC. *J Power Sources*. 2007;168:453–458.
23. Shao Z, Hsing I, Zhang H, Yi B. Influence of anode diffusion layer on the performance of a liquid feed direct methanol fuel cell by AC impedance spectroscopy. *Int J Energy Res*. 2006;30:1216–1227.
24. Leighton DT Jr, McCready MJ. Shear enhanced transport in oscillatory liquid membranes. *AIChE J*. 1988;34:1709–1712.
25. Chandhok AK, Voorhies N, McCready MJ, Leighton DT Jr. Measurement of transport enhancement in oscillatory liquid membranes. *AIChE J*. 1990;36:1259–1262.
26. Ye Q, Zhao TS, Xu C. The role of under-rib convection in mass transport of methanol through the serpentine flow field and its neighboring porous layer in a DMFC. *Electrochim Acta*. 2006;51:5420–5429.
27. Oliveira VB, Falcão DS, Rangel CM, Pinto AMFR. A comparative study of approaches to direct methanol fuel cells modelling. *Int J Hydrogen Energy*. 2007;32:415–424.
28. Koch DL, Brady JF. The effective diffusivity of fibrous media. *AIChE J*. 1986;32:575–591.
29. Speilman L, Goren SL. Model for predicting pressure drop and filtration efficiency in fibrous media. *Environ Sci Technol*. 1968;2: 279–287.
30. Gurau B, Smotkin ES. Methanol crossover in direct methanol fuel cells: a link between power and energy density. *J Power Sources*. 2002;112:339–352.
31. Wang ZH, Wang CY. Mathematical modeling of liquid-feed direct methanol fuel cells. *J Electrochem Soc*. 2003;150:A508–A519.
32. Lim C, Wang CY. Development of high-power electrodes for a liquid-feed direct methanol fuel cell. *J Power Sources*. 2003;113:145–150.
33. Batchelor GK. *An Introduction to Fluid Dynamics*. Cambridge: Cambridge University Press, 1967.
34. Walther C, Kühl H-D, Schultz S. Numerical investigations on the heat transfer in turbulent oscillating pipe flow. *Heat Mass Transfer*. 2000;36:135–141.
35. Landau LD, Lifshitz EM. *Course of Theoretical Physics*, *Volume 6*: *Fluid Mechanics*. Oxford: Pergamon Press, 1987.
36. Akhavan R, Kamm RD, Shapiro AH. An investigation of transition to turbulence in bounded oscillatory Stokes flows, Part 1: Experiments. *J Fluid Mechanics*. 1991;225:395–422.
37. Churchill SW. Friction-factor equation spans all fluid flow regimes. *Chem Eng*. 1977;84:91–92.
38. Ohmi M, Iguchi M. Flow patterns and frictional losses in an oscillating pipe-flow. *B JSME*. 1982;25:536–543.
39. Zhao TS, Cheng P. Experimental studies on the onset of turbulence and frictional losses in an oscillatory turbulent pipe flow. *Int J Heat Fluid Flow*. 1996;17:356–362.
40. Chan BC, Liu R, Jambunathan K, Zhang H, Chen G, Mallouk TE, Smotkin ES. Comparison of high-throughput electrochemical methods for testing direct methanol fuel cell anode electrocatalysts. *J Electrochem Soc*. 2005;152:A594–A600.
41. Argyropoulos P, Scott K, Taama WM. Gas evolution and power performance in direct methanol fuel cells. *J Appl Electrochem*. 1999; 29:661–669.
42. Argyropoulos P, Scott K, Taama WM. Carbon dioxide evolution patterns in direct methanol fuel cells. *Electrochim Acta*. 1999;44:3575–3584.

Manuscript received Apr. 26, 2007, and revision received Dec. 22, 2007.